SCIENCE CHINA
Chemistry

• ARTICLES •

doi: 10.1007/s11426-016-9009-6

Design, synthesis and biological evaluation of amino organophosphorus imidazoles as a new type of potential antimicrobial agents

Wei-Wei Gao[1], Syed Rasheed[1], VijaiKumarReddy Tangadanchu[1], Yi Sun[1], Xin-Mei Peng[1], Yu Cheng[1], Feng-Xiu Zhang[1], Jian-Mei Lin[2*] & Cheng-He Zhou[1*]

[1]*Institute of Bioorganic & Medicinal Chemistry, Key Laboratory of Applied Chemistry of Chongqing Municipality, School of Chemistry and Chemical Engineering, Southwest University, Chongqing 400715, China*
[2]*School of Medicine University of Electronic Science and Technology of China, Chengdu 610072, China*

Received December 1, 2016; accepted January 23, 2017; published online May 9, 2017

A series of amino organophosphorus imidazoles were designed and synthesized as a novel structural type of antimicrobial agents. Bioactive evaluation *in vitro* showed that compound **3f** exhibited equipotent or superior anti-methicillin-resistant *Staphylococcus aureus* (anti-MRSA) and anti-*S. cerevisiae* efficiencies (minimal inhibitory concentration (MIC)=2 μg/mL) to clinical drugs, and the combinations with antibacterial or antifungal drugs enhanced the antimicrobial efficiency. Highly active molecule **3f** showed low propensity for bacteria to develop resistance, and the preliminary action mechanism studies demonstrated that **3f** was membrane-active, but had no significant intercalation towards MRSA DNA. The computational study on **3f** reasonably explained its high antimicrobial activity. Experimental data revealed that ground-state **3f**-HSA complexes were formed mainly through hydrophobic interactions and hydrogen bonds with a spontaneous process, and the non-radioactive energy transfer from HSA to **3f** occurred beyond Förster resonance energy transfer theory. The participation of metal ions in **3f**-HSA supramolucular system could increase the concentration of free compound **3f**, and shorten its storage time and half-life in the blood to improve the maximum antimicrobial efficacy.

organophosphorus, imidazole, antibacterial, antifungal, HSA

Citation: Gao WW, Rasheed S, Tangadanchu VKR, Sun Y, Peng XM, Cheng Y, Zhang FX, Lin JM, Zhou CH. Design, synthesis and biological evaluation of amino organophosphorus imidazoles as a new type of potential antimicrobial agents. *Sci China Chem*, 2017, 60: doi: 10.1007/s11426-016-9009-6

1 Introduction

Multidrug-resistant pathogens like methicillin-resistant *Staphylococcus aureus* (MRSA), methicillin-resistant *Staphylococcus epidermidis* (MRSE) and vancomycin-resistant *Enterococcus faecium* (VRE), have become a major public health concern. Despite of a half century of efforts to find effective treatments, healthcare practitioners are still challenged to cure infections caused by resistant pathogens. In addition, both *Pseudomonas aeruginosa* and *Escherichia coli* also have shown rapid development of resistance against several classes of antibiotics that have been used for a long time [1]. As a result, many traditional antibiotics decrease or totally lose the effects and activities, and the use of antimicrobial drugs is being more and more limited. Thus, it is an increasingly active topic to develop antimicrobial agents with structural novelty and functional peculiarity for these Gram-positive and Gram-negative pathogens.

It is well known that heterocyclic imidazole plays an ex-

*Corresponding authors (email: linjianmei@med.uestc.edu.cn; zhouch@swu.edu.cn)

tremely important role in medicinal field, numerous imidazole derivatives as drugs have been used in clinic, especially in antimicrobial drugs such as the antibacterial Metronidazole, Ornidazole and Secnidazole as well as the antifungal Eniconazole, Miconazole and Sertaconazole (Figure 1) [2]. The imidazole nucleus has also been identified as an effective isostere of thiazole, oxazole, triazole, pyrazole, tetrazole, etc. in drug design, which strongly supports the large developmental value and spacious potentialities, and the exploitation of all possible application of imidazole-based compounds as medicinal drugs has been being one of the attracting highlighted topics. Numerous outstanding achievements have been revealed that imidazole nucleus in combination with antimicrobial moieties like quinolone, berberine, naphthalimide and sulfanilamide has wide potentiality in antimicrobial use [3]. However, the combination of the imidazole nucleus with organophosphorus fragments has been seldom observed. Therefore, it is importantly meaningful to combine the organophosphorus fragment with the imidazole core in order to investigate the contribution to antimicrobial activities.

Phosphorus element is ubiquitous in nature and plays positive roles in living organisms, and organophosphorus compounds have received much attention owing to their various bioactivities. Some of organophosphorus antimicrobial drugs have been widely used in clinic, such as the phosphonic acid derivatives Fosfomycin, Fosfomochlorin and Fosmidomycin behaving a broad spectrum of activities against a variety of Gram-positive and Gram-negative pathogens. Phosphonates are extensively used as prodrugs to improve biological activities through regulating solubility like prodrug Fosfluconazole, exhibiting better antifungal activity than Fluconazole (Figure 2) [4]. In spite of enormous potentiality of organophosphorus compounds against microbes, probably owning to the difficulty of synthetic methodology to access antimicrobial organophosphorus derivatives, the related work is relatively seldom. Thus, we have an overwhelming interest to develop organophosphorus imidazoles as novel antimicrobial agents with structural novelty and functional peculiarity.

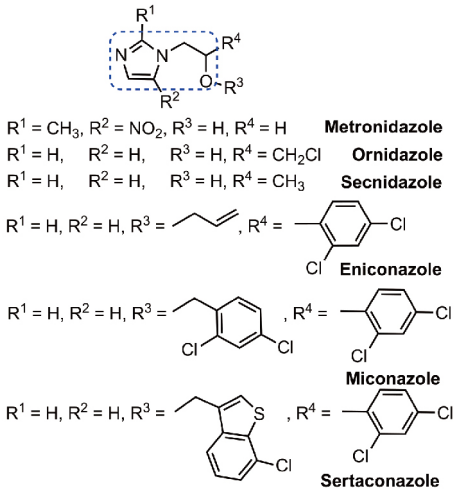

Figure 1 Structures of some antimicrobial imidazole compounds (color online).

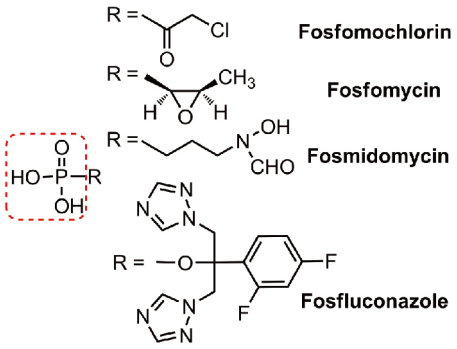

Figure 2 Structures of some antimicrobial organophosphorus compounds (color online).

In view of the above observations, as an extension of our research on bioactive heterocyclic compounds [5], herein a series of structurally novel compounds with a combination of amine, organophosphorus and imidazole nucleus as potentially antimicrobial agents were developed (Figure 3). The designed target compounds were based on the following considerations.

(1) The unique imidazole nucleus is a two-nitrogen five-numbered aromatic heterocycle, this type of structural fragment can readily accept or donate proton and exert various non-covalent interactions with the enzymes and receptors in organisms via coordination bonds, hydrogen bonds, ion-dipole, cation-π, π-π stacking, hydrophobic effect and van der Waals force etc., which helpfully modulates the pharmacokinetic properties. More importantly, imidazole nucleus can coordinate with a variety of inorganic metal ions to produce supramolecular complexes, which may not only exert the bioactivities of imidazoles themselves, but also exhibit the advantages of supramolecular complexes, possi-

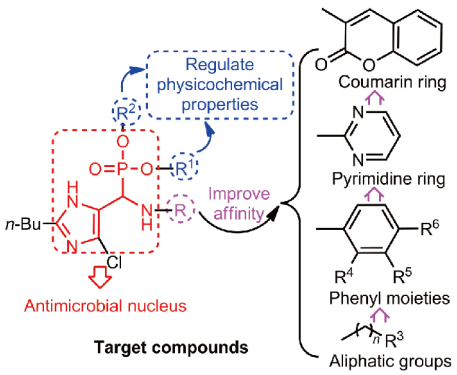

Figure 3 Design of novel organophosphorus imidazoles (color online).

bly exerting double action mechanisms to overcome the drug resistance [6]. Rationally, imidazole moiety is chosen as an important fragment of the target molecule.

(2) The organophosphorus group can provide unique binding interactions with biological targets because of their di- or trivalent chelating properties and possibly dual function as a hydrogen acceptor and donor at physiological pH [7]. Moreover, the introduction of organophosphorus moiety would play important roles in regulating the physicochemical properties of target molecules through changing the intermolecular forces and molecular polarity, then possibly improving the lipoid/water solubility. Therefore, the organophosphorous fragment was incorporated into the target molecules to discover new molecular scaffolds with high efficiency and lower resistance.

(3) Amino group is one of the most important moieties with prominent functionality in organic molecules, and 84% of small-molecule pharmaceuticals contain at least one [8]. It can target biomacromolecules in organisms to exhibit biological activity. Thus, it may be necessary to introduce amino group into the antimicrobial nucleus.

(4) The coordination properties of phosphorus and oxygen atoms in organophosphorus moiety or nitrogen atoms both in amino group and imidazole nucleus might make them form supramolecular complexes which could interact with DNA, HSA, enzymes, and other biomacromolecules to behave multi-targeting property.

(5) Aliphatic chain could significantly influence bioactivities through regulating the flexibility of molecules. Thus, alkyl organophosphorous imidazole **2** was prepared to explore the effect of aliphatic substituents on the antimicrobial activity.

(6) It is well known that the substituted aromatic ring can regulate the rigidity of target molecule, and substituents on benzene rings would improve the binding affinity to targets. In view of this, electron withdrawing and donating groups substituted phenyl organophosphorous imidazoles **3**, **4** and **5** were prepared with the aim to explore the effect of substituents on biological activity.

(7) Pyrimidine, an important aromatic hetertocycle with two nitrogen atoms, has been prevalently employed in drug design molecules for treating a variety of diseases [9]. Herein, the pyrimidine ring as a nitrogen containing moiety was introduced into the target molecule **6** to evaluate the antimicrobial activity.

(8) Coumarin has a rigid fused structure of benzene ring and α-pyrone, its derivatives exhibit extensively medicinal application and multi-targeting properties [10]. Herein, the coumarin moiety as a larger fragment was introduced into the target molecule **7** to investigate its effect on the antimicrobial activity.

All the newly synthesized compounds were evaluated for their antibacterial and antifungal activities *in vitro* against nine bacteria and five fungi. The pharmacokinetics properties including drug combination study, bactericidal kinetic assay and resistance investigation were done to further evaluate the biological activity of the most active molecule. Also, computational methods were used to predict these pharmacokinetic properties of the drug candidate and to rationalize its biological activity. The preliminary interactions between the highly active compound and calf thymus DNA or bacterial membrane were investigated to provide the possible binding mechanism and to make further help for the design, modification and screening of new drug molecules. Moreover, the effects of metal ions on their transportation by human serum albumin (HSA) were also investigated in order to preliminarily evaluate their transportation, distribution, and metabolism by fluorescence and UV-Vis absorption spectroscopy on molecular level.

2 Experimental

2.1 Synthesis

The procedures of synthesizing compounds **2–7** and **9** are provided in the Supporting Information online.

2.2 Biological assays

The *in vitro* minimal inhibitory concentrations (MICs) (in μg/mL) of the target compounds were determined using the two-fold serial dilution technique in 96-well microtest plates, according to the National Committee for Clinical Laboratory Standards (NCCLS) [11]. The tested microorganism strains were provided by the School of Pharmaceutical Sciences, Southwest University and the College of Pharmacy, Third Military Medical University, China.

2.2.1 Antibacterial assays

The prepared compounds **2a–2b**, **3a–3i**, **4a–4f**, **5a–5c**, **6** and **7** were evaluated for their antibacterial activities against four Gram-positive bacteria (*Staphylococcus aureus* ATCC25923, MRSA, *Micrococcus luteus* ATCC 4698 and *Bacillus subtilis* ATCC 21216), and five Gram-negative bacteria (*Escherichia coli* JM109, *Pseudomonas aeruginosa* ATCC 27853, *Bacillus proteus* ATCC 13315, *Eberthella typhosa* ATCC 14028 and *Shigella dysenteriae* ATCC 49550). The bacterial suspension was adjusted with sterile saline to a concentration of 1×10^5 CFU. The tested compounds were dissolved in dimethyl sulfoxide (DMSO) to prepare the stock solutions. The tested compounds and reference drugs were prepared in Mueller-Hinton broth (Guangdong Huaikai Microbial Sci.& Tech Co., Ltd., Guangzhou, China) by two fold serial dilution to obtain the required concentrations of 512, 256, 128, 64, 32, 16, 8, 4, 2, 1, 0.5 μg/mL. These dilutions were inoculated and incubated at 37 °C for 24 h. To ensure that the solvent had no effect on bacterial growth, a control test was performed with

test medium supplemented with DMSO at the same dilutions as used in the experiment. The MICs for **2a**–**2b**, **3a**–**3i**, **4a**–**4f**, **5a**–**5c**, **6** and **7** were summarized in Table1.

2.2.2 Antifungal assays

The newly synthesized compounds **2a**–**2b**, **3a**–**3i**, **4a**–**4f**, **5a**–**5c**, **6** and **7** were evaluated for their antifungal activities against *Candida albicans* ATCC 76615, *Candida utilis* ATCC 9950, *Candida mycoderma* ATCC 9888, *Saccharomyces cerevisiae* ATCC 9763 and *Aspergillus flavus* ATCC 204304. A spore suspension in sterile distilled water was prepared from a culture of the fungi growing on Sabouraud agar (SA) media, aged 1 d. The final spore concentration was 1×10^3–5×10^3 spore/mL. From the stock solutions of the tested compounds and reference antifungal drug Fluconazole, dilutions in sterile RPMI 1640 medium (Neuronbc Laboraton Technology CO., Ltd., Beijing, China) were made, resulting in eleven desired concentrations (0.5 to 512 μg/mL) of each tested compound. These dilutions were inoculated and incubated at 36 °C for 24 h.

2.2.3 Drug combination assays

The drug combination studies between the most active compound **3f** and standard drugs Chloromycin, Norfloxacin, Ciprofloxacin and Fluconazole were investigated by 2-fold dilution checkerboard assay method with concentration values from 1/32 to 4 times the MIC value of each molecule. The drug combination effect is usually expressed using frac-

Table 1 *In vitro* antibacterial data as MIC (μg/mL) for compounds **2**–**7** [a)]

Compounds	Gram-positive bacteria [b)]				Gram-negative bacteria [b)]				
	S. aureus	MRSA	*B. subtilis*	*M. luteus*	*E. coli*	*E. typhosa*	*S. dysenteriae*	*P. aeruginosa*	*B. proteus*
2a	16±2.4	16±2.4	128±25.6	64±9.6	256±38.4	256±38.4	256±0.0	16±2.4	64±9.6
2b	16±2.4	32±6.4	128±0.0	128±25.6	256±38.4	128±25.6	128±25.6	64±9.6	128±25.6
3a	32±6.4	32±2.4	32±6.4	16±2.4	16±2.4	64±0.0	32±6.4	4±1.2	16±2.4
3b	64±9.6	8±1.6	64±3.6	64±9.6	128±25.6	128±9.6	32±6.4	4±0.2	32±6.4
3c	32±0.0	16±2.4	128±25.6	16±2.4	128±25.6	64±9.6	128±25.6	64±9.6	64±9.6
3d	128±25.6	64±9.6	128±25.6	64±0.0	256±0.0	256±38.4	32±6.4	4±1.2	128±25.6
3e	128±9.6	128±25.6	128±25.6	64±3.6	16±0.0	64±6.4	256±25.6	16±2.4	128±0.0
3f	8±0.0	2±0.8	32±6.4	32±0.0	16±2.4	32±0.0	16±2.4	2±0.0	16±2.4
3g	128±25.6	32±6.4	128±25.6	64±9.6	32±6.4	256±9.6	256±0.0	16±2.4	32±6.4
3h	32±6.4	128±25.6	256±0.0	64±6.4	512±38.4	256±38.4	256±38.4	32±2.4	128±25.6
3i	128±25.6	128±9.6	256±38.4	256±25.6	256±38.4	512±0.0	256±38.4	128±25.6	256±38.4
4a	64±9.6	128±25.6	256±0.0	128±25.6	256±0.0	256±38.4	128±25.6	64±9.6	256±38.4
4b	128±25.6	256±0.0	128±25.6	128±25.6	256±38.4	128±25.6	256±38.4	128±9.6	128±25.6
4c	128±25.6	128±25.6	256±0.0	128±9.6	128±25.6	64±9.6	128±25.6	64±9.6	128±25.6
4d	64±3.6	128±25.6	128±25.6	256±38.4	128±25.6	128±25.6	256±38.4	128±25.6	64±9.6
4e	128±25.6	128±25.6	64±9.6	256±0.0	256±38.4	128±25.6	64±6.4	128±25.6	128±25.6
4f	128±9.6	64±9.6	128±25.6	128±25.6	128±25.6	256±0.0	128±25.6	128±25.6	64±6.4
5a	128±25.6	128±25.6	256±0.0	256±38.4	128±0.0	512±0.0	128±25.6	4±1.2	128±25.6
5b	64±9.6	128±25.6	128±25.6	64±0.0	128±25.6	256±38.4	64±9.6	4±1.2	64±9.6
5c	64±6.4	128±25.6	256±38.4	128±25.6	128±0.0	256±0.0	32±6.4	8±1.6	128±25.6
6	32±6.4	32±6.4	128±25.6	128±25.6	128±25.6	256±0.0	256±38.4	16±0.0	64±9.6
7	32±6.4	64±0.0	256±38.4	128±25.6	256±38.4	256±38.4	256±38.4	8±1.6	128±0.0
A [c)]	16±2.4	16±2.4	32±6.4	8±0.0	32±6.4	32±6.4	32±0.0	32±6.4	32±6.4
B [c)]	0.5±0.0	8±1.6	1±0.0	2±0.2	16±2.4	4±0.0	4±1.2	16±2.4	8±1.6
C [c)]	4±1.2	2±0.0	2±0.8	4±0.0	1±0.2	2±0.0	0.5±0.0	0.5±0.0	2±0.0

a) Minimal inhibitory concentrations were determined by micro broth dilution method for microdilution plates, and the data are average of multiple replicates. b) *S. aureus*, *Staphylococcus aureus* (ATCC 25923); MRSA, methicillin-resistant *Staphylococcus aureus* (N315); *B. subtilis*, *Bacillus subtilis* (ATCC 21216); *M. luteus*, *Micrococcus luteus* (ATCC 4698); *E. coli*, *Escherichia coli* (JM109); *E. typhosa*, *Eberthella typhosa* (ATCC 14028); *S. dysenteriae*, *Shigella dysenteriae* (ATCC 49550); *P. aeruginosa*, *Pseudomonas aeruginosa* (ATCC 27853); *B. proteus*, *Bacillus proteus* (ATCC 13315). c) **A**=Chloromycin; **B**=Norfloxacin; **C**=Ciprofloxacin.

tional inhibitory concentration (FIC) index. The FIC value can be calculated as FIC=MIC of compound A in mixture/MIC of compound A alone+MIC of compound B in mixture/MIC of compound B alone. Using this method, FIC≤0.5 represents synergism; FIC>0.5 and ≤1.0 represents additivism; FIC>1 and ≤2 represents an indifferent effect; and FIC>2 represents antagonism.

2.2.4 Resistance assays

Both strains of *S. aureus* and MRSA were exposed to sub-MICs of compound **3f** for sustained passages, and then the MIC of compound **3f** was determined against each passage of the strains. The freshly diluted *S. aureus* and MRSA strains (1.0×10^5 CFU) in the broth medium were cultured in 1.3 μg/mL (2/3 MIC) of compound **3f** at 37 °C for 12 h on a shaker bed at 90 r/min, and the sensitivity of each strain passage to compound **3f** was tested. To make comparative analysis, parallel cultures were exposed to 2-fold dilutions with the reference drugs Chloromycin, Norfloxacin and Ciprofloxacin as positive controls.

2.2.5 Bactericidal kinetic assays

The rate of which the compound killed bacteria was evaluated by performing time-kill kinetics. MRSA was cultured in suitable medium at 37 °C for 6 h and diluted in respective media. Compound **3f** was added to the bacterial solution (MRSA of approximately 1.8×10^5 CFU/mL) at concentration of 4×MIC in a 96-well plate. The plate was then incubated at 37 °C. At different time intervals (0, 60, 90, 120, 150, 180, 210, 240, 300 and 360 min), 20 μL of aliquots from the solution were taken out and serially diluted (10-fold serial dilution) in 0.9% saline. Then 20 μL of the dilutions was plated on respective agar plates and incubated at 37 °C for 24 h. The bacterial colonies were counted, and results represented in logarithmic scale: $\log_{10}$ (CFU/mL) vs. time (in min).

2.2.6 Bacterial membrane permeabilization assays

The 6 h grown culture (mid log phase) of MRSA and *P. aeruginosa* was harvested (3500 r/min, 5 min), washed, and resuspended in 5 mM glucose and 5 mM HEPES buffer (pH 7.2) in 1:1 ratio. Then an amount of 10 μL of tested compound **3f** (12×MIC) was added to a cuvette containing 2 mL of bacterial suspension and 10 μM propidium iodide (PI). Fluorescence was monitored at excitation wavelength of 535 nm (slit width of 10 nm) and emission wavelength of 617 nm (slit width of 5 nm). As a measure of inner membrane permeabilization, the uptake of PI was monitored by the increase in fluorescence for 2 h.

3 Results and discussion

3.1 Chemistry

A series of amino organophosphorus imidazoles were conveniently synthesized according to the synthetic route outlined in Scheme 1. Alkyl imidazoles **2a** and **2b** were prepared in

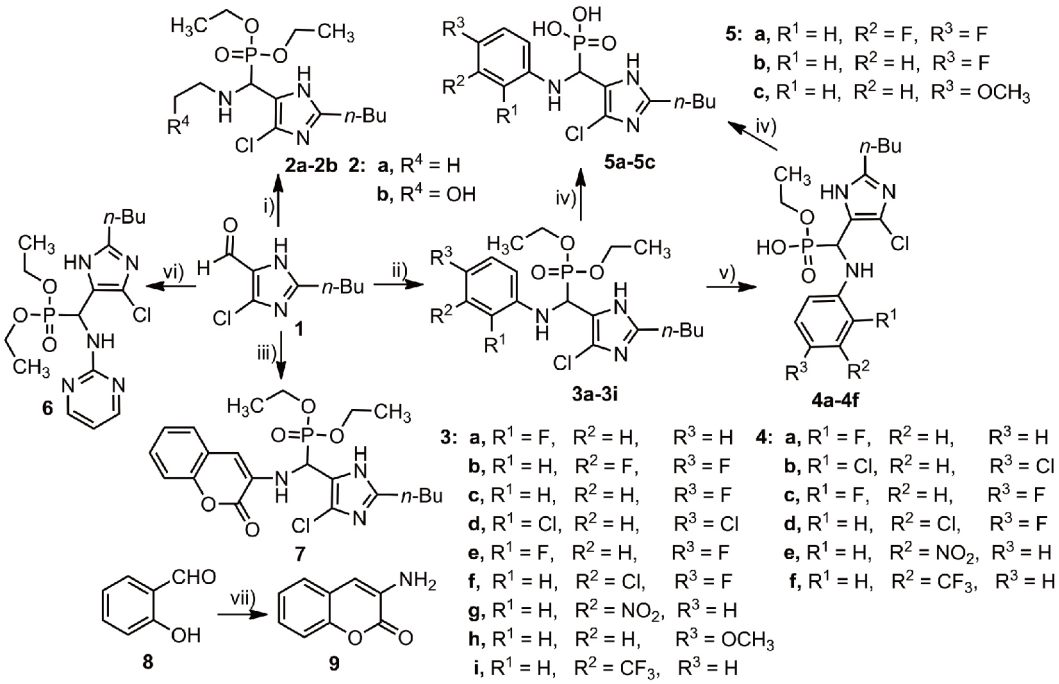

Scheme 1 The synthetic route of amino organophosphorus imidazoles. Reagents and conditions are: i) diethyl phosphonate, aliphatic amines, toluene, reflux; ii) diethyl phosphonate, phenyl amines, toluene, reflux; iii) diethyl phosphonate, 3-amino-2*H*-chromen-2-one, toluene, reflux; iv) conc. hydrochloric acid, 80 °C; v) conc. hydrochloric acid, 50 °C; vi) diethyl phosphonate, pyrimidin-2-amine, toluene, reflux; vii) methyl glycinate hydrochloride, Et_3N, 30 min, 90 °C, pH 9–10.

yields of 50% and 49% from commercially available 2-butyl-4-chloro-1*H*-imidazole-5-carbaldehyde, diethyl phosphonate and aliphatic amines in toluene. Phenyl type of imidazole compound **3** was obtained in 60%−80% yields under the same reaction condition starting from a series of anilines, and then further hydrolyzed in concentrated hydrochloric acid to afford imidazole phosphonic acids **4** and **5** with yields ranging from 40% to 60%. Pyrimidine-based molecule **6** was obtained under the same reaction condition starting from 2-aminopyrimidine in the yield of 50%. Coumarin derivative **7** was efficiently synthesized in good yield by the Mannish reaction of 3-aminocoumarin which was easily prepared from the one-pot cyclization of 2-hydroxyl benzaldehyde and methyl glycinate hydrochloride. The HPLC analysis showed that almost all of the prepared target compounds were pure, and the related HPLC spectra were provided in the Supporting Information online.

3.2 Spectral analysis

All the newly synthesized target imidazol phosphonates and imidazol phosphonic acids were characterized by infrared spectroscopy (IR), nuclear magnetic resonance of ^{1}H (^{1}H NMR), ^{13}C NMR, ^{31}P NMR and high resolution mass spectrometry (HRMS). The spectral analyses were in accordance with the assigned structures, and all the spectral data were listed in the experimental protocols. The HRMS for each new compounds gave a major fragment of $[M+H]^+$ or $[M+Na]^+$ according to their molecular formula.

3.2.1 IR spectra

Almost all the target compounds gave similar IR spectra and there was no large difference for the characteristic absorption peaks. Characteristic NH stretching bands were observed between 3361 and 3302 cm^{-1}. In addition, three sharp and strong peaks at 2970–2957 cm^{-1}, 2935–2931 cm^{-1} and 2875–2866 cm^{-1} were ascribed to the vibration of aliphatic C−H bonds. The stretching of P=O groups showed frequencies around 1250–1218 cm^{-1}. The characteristic absorption peaks of aromatic frame for imidazole phosphonates **3**, **6** and **7**, imidazole phosphonic acids **4** and **5** appeared in the region of 1650–1450 cm^{-1}, and the broad absorption around 3445–3394 cm^{-1} was attributed to the P–OH group in compounds **4** and **5**. All the other absorption bands were also observed at expected regions.

3.2.2 ^{1}H NMR spectra

In ^{1}H NMR spectra, it was noticed that the protons of secondary amine appeared sometimes, Im-NH and Ph-NH existed as single peak in δ 11.07–11.47 ppm and δ 5.06–5.95 ppm, respectively. Most of the protons of hydroxyl group in imidazole phosphonic acids **4** and **5** did not appear at all. For imidazole phosphonates **2**, **3**, **6** and **7**, the chemical shifts of P–OCH_2 were different, and there were three or four signals for P–OCH, P–OCH and P–OCH_2 in δ 3.87–4.12 ppm, 3.75–4.02 ppm and 4.16–4.37 ppm, respectively, due to the adjacency of chiral carbon. The chemical shifts for the protons of chiral carbon of all the targets as double peaks in δ 4.16–5.06 ppm. The signals of the aromatic protons appeared ranging from 6.36 ppm to 7.59 ppm. The aromatic protons showed various multiplicities such as doublets due to several couplings and the influence of F atom. The ^{1}H resonances of aliphatic groups such as CH_2 and CH_3 were observed in the region between 2.83 and 0.78 ppm mainly influenced by the imidazole ring, because of the effect of electron-withdrawing imidazole ring, the protons of CH_2 linked to 2-position gave large downfield chemical shifts around δ 2.41–2.83 ppm.

3.2.3 ^{13}C NMR spectra

The ^{13}C NMR spectra of all the target imidazole phosphonates and imidazole phosphonic acids were consistent with the assigned structures. No large difference was found in ^{13}C chemical shifts for the chiral carbon and 2-, 4-, 5-position of imidazole ring. The impalpable distinctions of some chemical shifts were mainly attributed to the substituent at different positions of aromatic carbons and to the various amines. Additionally, all the aliphatic carbons appeared at the appropriate chemical shift regions.

3.2.4 ^{31}P NMR spectra

There was only one signal peak in each ^{31}P NMR spectrum of all the target compounds. For imidazole phosphonates **2**, **3**, **6** and **7**, the chemical shifts were almost in δ 18.95–21.60 ppm, but for imidazole phosphonic acids **4**, δ 12.99–20.13 ppm, and for compound **5**, δ 16.23–18.17 ppm due to the adjacency of hydroxyl group.

3.3 Biological activity

3.3.1 Antibacterial activity

The antibacterial assay showed that some target compounds exhibited moderate to good efficacy against some tested bacterial strains (Table 1). Noticeably, compound **3f** with 3-chloro-4-fluorophenyl group was the most active molecule, which deserved to be further investigated as potentially antimicrobial agent.

Table 1 showed that the phenyl series of compound **3** exhibited moderate to good activities against Gram-negative bacteria *P. aeruginosa* with MIC values of 4–32 μg/mL, except for 4-fluorophenyl derivative **3c** (MIC=64 μg/mL) and 3-trifluoromethylphenyl compound **3i** (MIC=128 μg/mL). Compound **3a** with 2-fluorophenyl moiety gave a MIC value of 16 μg/mL against *E. coli*, which was superior to Chloromycin (MIC=32 μg/mL) and equipotent to Norfloxacin (MIC=16 μg/mL). 3,4-Difluorophenyl derivative **3b** showed good activity against MRSA with MIC

value of 8 μg/mL, which was better than Chloromycin (MIC=16 μg/mL) and almost equipotent to Norfloxacin (MIC=8 μg/mL). Compounds **3g** and **3h** with non-halo substituted benzene rings only possessed acceptable anti-*P. aeruginosa* activities with MIC values of 16 and 32 μg/mL, respectively. Moreover, 3-chloro-4-fluorophenyl derivative **3f** exhibited superior activity against Gram-negative strains *E. coli* (MIC=16 μg/mL), *S. dysenteriae* (MIC=16 μg/mL), *P. aeruginosa* (MIC=2 μg/mL) and *B. proteus* (MIC=16 μg/mL) to Chloromycin (MIC=32 μg/mL). It also possessed superior anti-MRSA (MIC=2 μg/mL) efficiency to Chloromycin (MIC=16 μg/mL) and Norfloxacin (MIC=8 μg/mL), and almost equipotent to Ciprofloxacin (MIC=2 μg/mL). These implied that compound **3f** exhibited moderate to good efficacy with MIC values between 2 and 32 μg/mL, and behaved large potentiality with a broad antibacterial spectrum. However, the hydrolyzed imidazole phosphoric acids **5a**–**5c** exhibited decreased activities in comparison to the corresponding imidazole phosphonates against the tested bacterial strains, and they only showed moderate anti-*P. aeruginosa* efficacy with MIC values of 4−8 μg/mL. The corresponding phosphoric acid monoesters **4a**–**4f** almost possessed moderate antibacterial efficacies against all the tested bacterial strains, which might result from its decreased liposolubility after hydrolysis. Alkyl-derived molecules **2a** and **2b** with ethyl and hydroxyethyl groups also exhibited equipotent anti-*S. aureus* efficacy (MIC=16 μg/mL) to Chloromycin, while pyrimidine derivative **6** with heterocycle or coumarin one **7** with larger skeleton in contrast with phenyl derivative **3** only displayed moderate activity against *P. aeruginosa* with MIC value of 16 and 8 μg/mL, respectively. More work is necessary to elucidate them on antibacterial activity.

3.3.2 Antifungal activity

The antifungal data in Table 2 revealed that all target compounds displayed moderate inhibition activities against five tested fungi. The antifungal abilities for the synthesized compounds were similar to their antibacterial efficiencies. It was obviously found that all target compounds possessed anti-*A. flavus* activities with MIC values of 32–256 μg/mL, which were equipotent or superior to Fluconazole (MIC=256 μg/mL). Compounds **3a** and **3b** exhibited equipotent efficiencies against *C. utilis* to Fluconazole (MIC=8 μg/mL), and **3b** gave 4-fold better anti-*S. cerevisiae* activity than Fluconazole (MIC=16 μg/mL). Moreover, 3-chloro-4-fluorophenyl deriv-

Table 2 *In vitro* antifungal data as MIC (μg/mL) for compounds **2**–**7** [a)]

Compounds	*C. albicans*	*C. mycoderma*	*C. utilis*	*A. flavus*	*S. cerevisiae*
2a	256±38.4	64±6.4	16±2.4	128±25.6	256±0.0
2b	128±25.6	64±9.6	64±9.6	128±25.6	256±38.4
3a	64±9.6	128±0.0	8±1.6	32±6.4	32±6.4
3b	128±25.6	128±25.6	8±1.6	128±25.6	4±1.2
3c	64±9.6	64±9.6	16±0.0	128±9.6	128±25.6
3d	128±25.6	32±6.4	128±25.6	128±25.6	128±0.0
3e	512±76.8	64±9.6	256±38.4	64±0.0	256±38.4
3f	128±25.6	32±6.4	8±1.6	32±6.4	2±0.8
3g	512±76.8	64±9.6	128±0.0	64±9.6	128±25.6
3h	256±38.4	128±25.6	32±6.4	256±38.4	256±0.0
3i	512±0.0	256±0.0	64±9.6	256±0.0	32±6.4
4a	128±25.6	256±0.0	128±25.6	256±38.4	64±9.6
4b	512±76.8	256±38.4	64±9.6	128±0.0	128±25.6
4c	256±38.4	128±25.6	128±25.6	64±9.6	128±0.0
4d	128±25.6	64±9.6	128±25.6	128±25.6	256±38.4
4e	128±0.0	128±25.6	256±0.0	128±25.6	64±6.4
4f	64±9.6	128±25.6	128±25.6	64±0.0	64±9.6
5a	256±38.4	256±0.0	16±2.4	256±38.4	128±25.6
5b	128±25.6	128±25.6	32±6.4	64±9.6	256±0.0
5c	256±0.0	32±6.4	128±25.6	256±38.4	32±6.4
6	128±25.6	256±38.4	64±6.4	128±25.6	128±25.6
7	256±38.4	128±25.6	16±2.4	256±0.0	256±38.4
D [b)]	1±0.0	4±0.0	8±1.6	256±38.4	16±2.4

a) *C. albicans*, *Candida albicans* (ATCC 76615); *C. mycoderma*, *Candida mycoderma* (ATCC 96918); *C. utilis*, *Candida utilis*; *A. flavus*, *Aspergillus flavus*; *S. cerevisiae*, *Saccharomyces cerevisiae* (ATCC 9763); the data are average of multiple replicates. b) **D**=Fluconazole.

ative **3f** exhibited significant inhibition activity against *S. cerevisiae* with MIC value of 2 μg/mL, which was 8-fold more potent than Fluconazole.

The above discussion implied that the antimicrobial efficacies should be closely related to substituents on amines to some extent. Phenyl derivatives seemed to be more active than those of aliphatic chain, pyrimidine and coumarin rings, halo-substituted phenyl groups resulted in more potent against the tested strains than those of non-halo substituted ones, and both the extremely strong electron withdrawing groups such as nitro and trifluoromethyl ones and the electron donating groups like methoxyl one were unfavourable to some extent. Phosphonates seemed to be better than their hydrolyzed ones, it might be due to a relative decrease in liposolubility after hydrolysis.

3.3.3 Drug combination study

Much research has shown that the combination therapy in clinic with two or more agents might improve the efficiency and bioavailability, reduce or even eliminate side effects and allergic reactions and overcome multi-drug resistances as well as treat mixed diseases which cannot be cured by single drug [12]. The drug combination use between the most active molecule **3f** and clinical Chloromycin, Norfloxacin, Ciprofloxacin and Fluconazole were investigated. Most of the combinations of **3f** with Chloromycin, Norfloxacin, and Ciprofloxacin showed excellent antibacterial efficacy with less dosage and broad antimicrobial spectrum (Table 3). The FIC index was no more than 1.0, which meant that the combinations had excellent synergistic or additive effects. Except for the combination use of **3f** with both Chloromycin and Norfloxacin against *B. subtilis*, the FIC index was more than 1.0, which represented an indifferent effect. It was worthy to note that the combination of **3f** with clinical drugs could effectively inhibit the growth of MRSA. These results manifested that the combinations of compound **3f** with antibacterial drugs could enhance antibacterial activity, overcome drug resistance and broaden antibacterial spectrum.

The combination of Fluconazole with compound **3f** displayed good activities against fungi *C. utilis*, *A. flavus* and *S. cerevisia* with the FIC index being no more than 1.0 (Table 4). But the combination use of **3f** with Fluconazole against *C. albicans* and *C. mycoderma* produced the indifferent effect. Moreover, these combinations gave high activities with less dosage against Fluconazole-insensitive *A. flavus*. It clearly showed that the combination of Fluconazole with **3f** broadened antifungal spectrum.

3.3.4 Resistance study

Resistance to antibiotics has been increasing in recent years and becoming a serious and global challenge to the chemotherapy or drug discovery. The mutagenic properties of bacteria raise the possibility of the resistance even in smaller populations of bacteria exposed to low concentration of antibacterial drugs, which may promote the ease of selection of low-level resistance mutations [13]. Therefore, it is significantly vital to study the resistance of the potent compound against bacterial strains. To investigate the drug resistance of compound **3f**, the susceptible Gram-positive pathogens *S. aureus* and MRSA, Gram-negative strain *P. aeruginosa* were employed, and Chloromycin, Norfloxacin, Ciprofloxacin as positive control. The experimental results (Figure 4) showed that the low propensity of both Gram-positive and Gram-negative bacteria to develop resistance against 3-chloro-4-fluorophenyl derivative **3f** as there was almost no or little change in the MIC values even after 12 passages.

3.3.5 Bactericidal kinetic study

The bactericidal efficiency for the highly active compound **3f** was also evaluated against MRSA by time-kill kinetics exper-

Table 3 Drug combinations of compound **3f** with antibacterial drugs Chloromycin, Norfloxacin and Ciprofloxacin [a)]

Bacteria	Chloromycin			Norfloxacin			Ciprofloxacin		
	Compound **3f** MIC (μg/mL)	Effect	FIC index	Compound **3f** MIC (μg/mL)	Effect	FIC index	Compound **3f** MIC (μg/mL)	Effect	FIC index
S. aureus	0.25±0.04	additivism	0.531	0.25±0.04	additivism	0.531	0.25±0.04	synergism	0.094
MRSA	0.12±0.02	additivism	0.562	0.062±0.01	synergism	0.281	0.062±0.01	synergism	0.039
B. subtilis	2±0.8	indifference	1.062	1±0.3	indifference	1.031	1±0.3	synergism	0.156
M. luteus	2±0.8	synergism	0.187	2±0.8	synergism	0.187	1±0.3	synergism	0.094
E. coli	1±0.3	synergism	0.187	0.5±0.2	synergism	0.156	1±0.3	synergism	0.312
E. typhosa	8±1.6	synergism	0.500	4±1.2	additivism	0.625	1±0.3	synergism	0.047
S. dysenteriae	2±0.8	synergism	0.250	2±0.8	additivism	0.625	0.5±0.2	synergism	0.281
P. aeruginosa	0.12±0.02	synergism	0.125	0.12±0.02	synergism	0.125	0.25±0.04	synergism	0.249
B. proteus	2±0.8	additivism	0.625	0.5±0.2	synergism	0.156	0.5±0.2	synergism	0.094

a) Average of multiple replicates.

Table 4 Drug combinations of compound **3f** with antifungal drug Fluconazole [a)]

Fungi	MIC (μg/mL)	Effect	FIC index
C. albicans	4±1.2	indifference	1.031
C. mycoderma	4±1.2	indifference	1.125
C. utilis	1±0.3	synergism	0.375
A. flavus	1±0.3	additivism	0.531
S. cerevisiae	0.25±0.04	synergism	0.375

a) Average of multiple replicates.

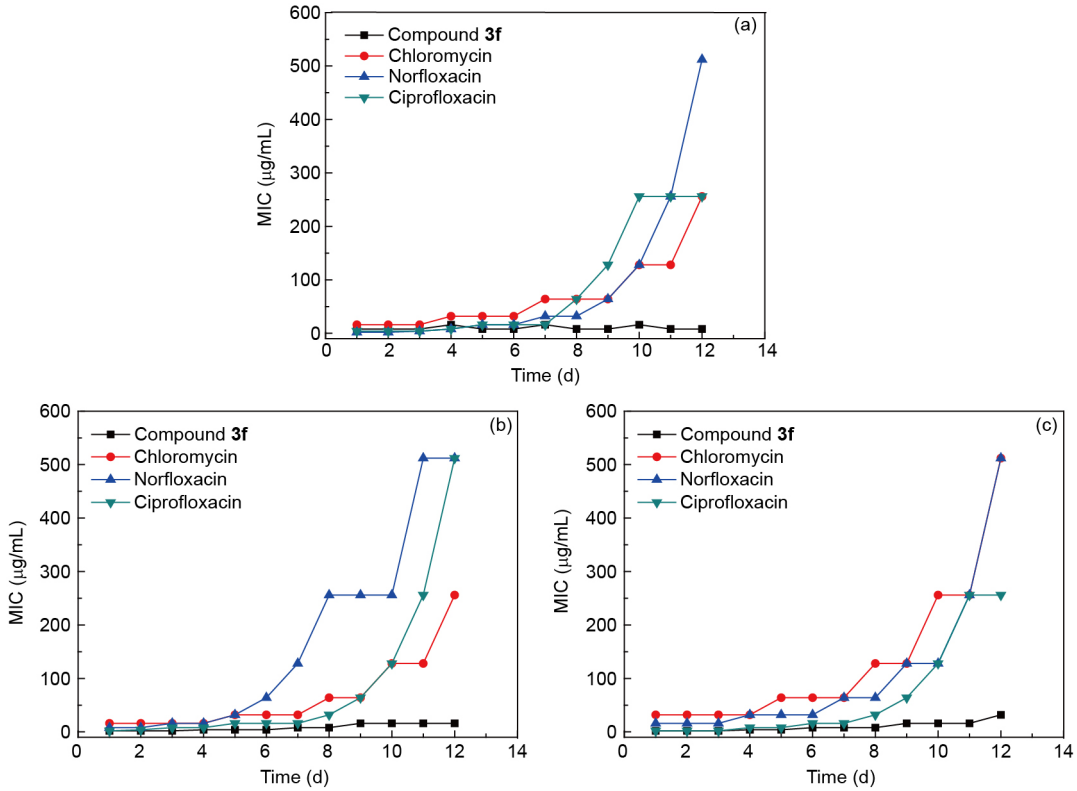

Figure 4 Evaluation of resistant development against compound **3f** in bacterial strains *S. aureus* (ATCC 25923) (a), MRSA (N 315) (b) and *P. aeruginosa* (ATCC 27853) (c) (color online).

iment. Figure 5 revealed nearly 10^3 CFU/mL reduction in the number of viable bacteria within 60 min at a concentration of 4-times MIC. The result manifested that **3f** had rapidly killing effect against MRSA [14].

3.3.6 Bacterial membrane permeabilization study

Bacterial membrane has been considered as an important and intriguing antibacterial target, and membrane-active nature induces low propensity for bacteria to develop resistance. Therefore, it is reasonable to speculate that antibacterial agents would have satisfactory efficacy and low drug-resistance if they target on or interact with cell membrane. Herein, the most active antimicrobial compound **3f** was chosen to investigate its membrane permeabilization against MRSA and *P. aeruginosa* bacteria by fluorescence spectra using propidium iodide (PI), a common dye that only can pass through the membrane of compromised cells and fluoresces

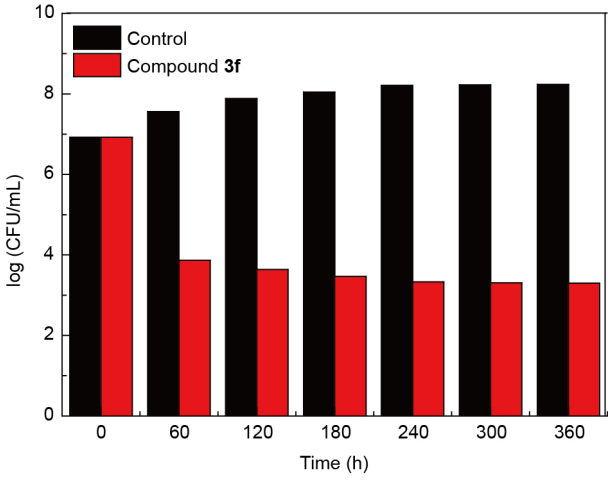

Figure 5 Bactericidal kinetics of compound **3f** at 4× MIC against MRSA (color online).

upon binding to the DNA [15]. For the increase of fluorescence intensity within 90 min in Figure 6, which might be due to the formed PI-DNA complexes as the gradual damage of bacterial membrane in the presence of **3f** at 12-times MIC. Also, the number of viable bacteria was nearly decreased by 6 log CFU/mL within 150 min at a concentration of 12-times MIC (Figure 7). These results manifested that compound **3f** could effectively interact with the membranes of both Gram-positive (MRSA) and Gram-negative (*P. aeruginosa*) bacteria.

3.4 Interactions with calf thymus DNA

In order to explore the possible antimicrobial action mechanism, the binding behavior of compound **3f** with calf thymus DNA was studied on molecular level *in vitro* using NR dye as a spectral probe by UV-Vis spectroscopic methods (Figure S1 and Figure S2, Supporting Information online). However, the maximum absorption peak of DNA at 260 nm exhibited no noticeable increase with the increasing concentration of compound **3f**. Besides, the absorption spectra of competitive interactions of **3f** and NR with DNA showed that the maximum absorption around 530 nm of the DNA-NR complexes did not decrease with the addition of **3f**, and no intensity increase was observed in the developing band around 460 nm. These meant that there was no remarkable intercalation towards calf thymus DNA or very weak interaction between **3f** and calf thymus DNA. The further investigation like its test toward MRSA DNA cleavage is necessary to explore the possible antimicrobial action mechanism.

3.5 Partition coefficient and computational analysis

The partition coefficient is used to define the lipophilic character of a drug, and the suitable values would make contribution to ideal pharmacokinetic and pharmacodynamic properties of drugs. In general, most of the target compounds (Figure 8) were lipophilic (*c*log*P*=1.33–5.17). The *c*log*P* values of phenyl series of compounds **3a**–**3i** were related to types of substituents on the benzene rings. The chloro group containing derivatives generally showed greater lipophilicity than fluoro, nitro or methoxyl group containing ones. Moreover, alkyl imidazoles **2**, imidazole phosphonic acids **4** and **5**, and pyrimidine-based molecule **6** possessed lower *c*log*P* values than phenyl imidazoles **3**, except for **4b** and **4f**. Compound **2b** with a hydroxyethyl group had the lowest *c*log*P* value. Molecules **3b**, **3d** and **3f** with relatively higher *c*log*P* values showed better antibacterial and antifungal activities in comparison with other target compounds. These might be responsible for the possibility that higher lipophilic compounds

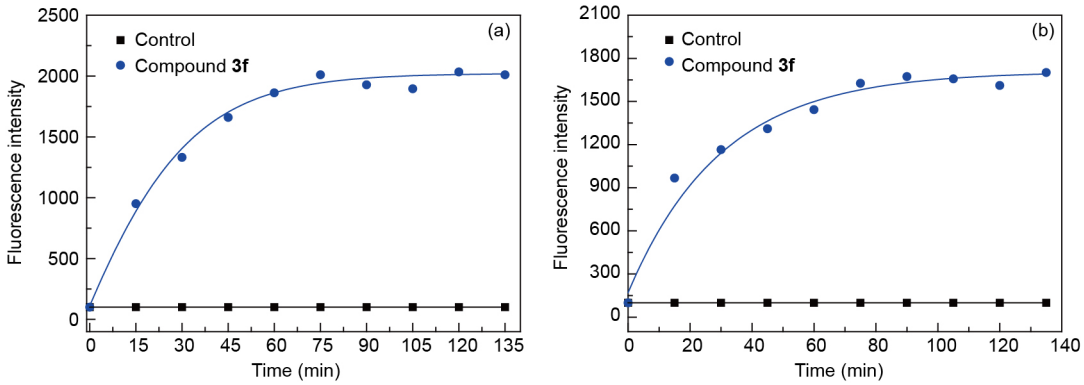

Figure 6 Bacterial membrane permeabilization of compound **3f** at concentrations of 12× MIC. (a) Against MRSA; (b) against *P. aeruginosa* (color online).

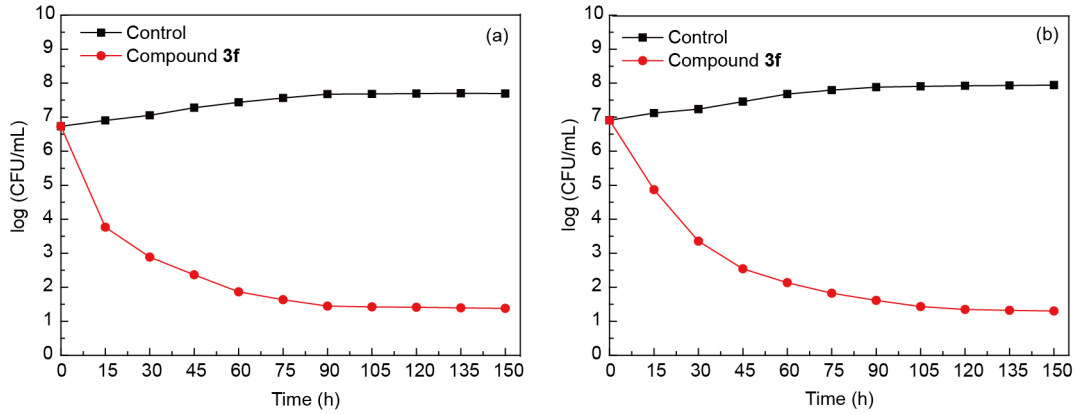

Figure 7 The growth curves of MRSA (a) and *P. aeruginosa* (b) in the presence of compound **3f** at 12-times MIC (color online).

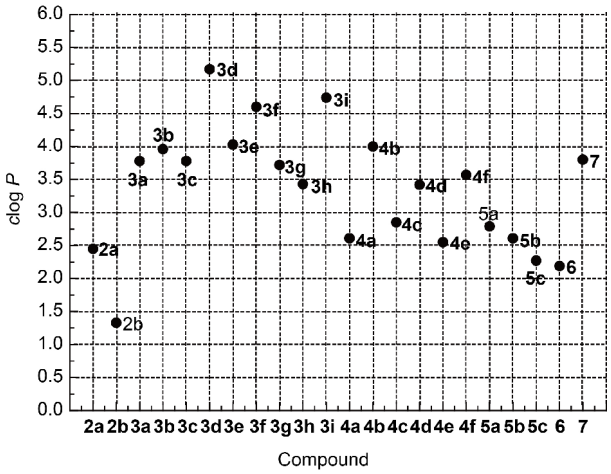

Figure 8 *c*log*P* values of compounds **2a**–**2b**, **3a**–**3i**, **4a**–**4f**, **5a**–**5c**, **6**, and **7** (color online).

were easy to be delivered to the binding sites.

Computational methods are usually used to predict important pharmacokinetic properties of drug candidates and to rationalize biological activity. The frontier molecular orbitals (FMO) theory, that is the highest occupied molecular orbital (HOMO) and the lowest unoccupied molecular orbital (LUMO) can always dominate the intermolecular interactions. As shown in Table 5, the plots of HOMOs and LUMOs of the most active compound **3f** and its structurally similar compound **3b** were obtained to analyze the main atomic contributions for these orbitals. The HOMOs of **3f** and **3b** were mainly focused on imidazole ring, halo-substituted benzene ring, chiral carbon, phosphoryl (P=O) and P–O groups, which indicated that those rings and groups might be active sites and the intermolecular interactions could take place between these sites and positively charged molecules. It was also found that the *n*-Bu on imidazole ring and ethyl groups of phosphonates did not contribute directly to the HOMO, manifesting that these groups might mainly adjust the physicochemical properties. In addition, the LUMOs of **3f** and **3b** were mainly located in the halo-substituted benzene ring which did good nucleophilic attack.

The molecular electrostatic potential (MEP) surface gives an indication of the charged surface area, an idea for explaining the hydrophilicity of compounds and the orientation of drug candidates for their activities [16]. Thus, MEP maps were given to investigate the similarities and differences in electrostatic binding characteristic of the surfaces of the most active antimicrobial **3f** and the less active one **3b** (Table 5). Comparing the MEP surfaces of **3f** and **3b** revealed that both of them had almost the same electropositive regions (in blue) but different electronegative regions (in red). The electronegative region mainly located on one P–O and the P=O groups in compound **3b**, while the electronegative region of **3f** moved towards the imidazole ring, which might be influenced by the chlorine atom on the benzene ring. This moving would be in favor of orientating drug candidate **3f** towards better biological activity, which indicated that the possible formation of hydrogen bonds with a share of N1-position of imidazole ring and the oxygen atom of P–O or P=O group. Therefore, it reasonably explained that compound **3f** possessed better biological activity than its analog **3b**.

3.6 Interactions of compound 3f with HSA

HSA is the principal extracellular protein in the circulatory system, and the distribution, metabolism, and efficacy of drugs can be changed by their affinity to HSA. Many promising new drugs have been rendered to be ineffective because of their unusually high affinity to this protein. So the investigation of interactions between drugs or bioactive small molecules and HSA is not only significant to design, modify and screen drug molecules but also helpful to understand the pharmacokinetic properties of drugs. Herein, highly active molecule **3f**-albumin binding was investigated by UV-Vis absorption and fluorescence spectra on the molecular level to

Table 5 Plots of the HOMOs, LUMOs and MEP maps of compounds **3f** and **3b** (color online)

Compounds	Simulation structures	HOMO	LUMO	MEPs
3f	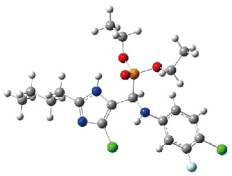	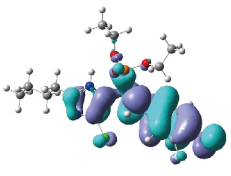	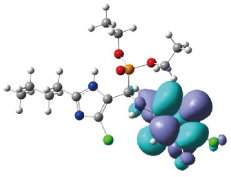	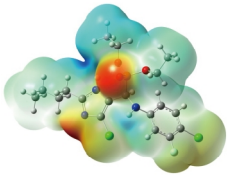
3b	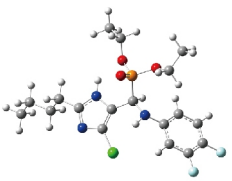	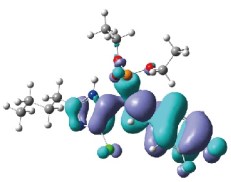	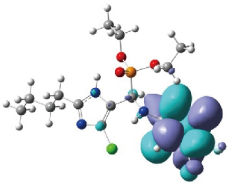	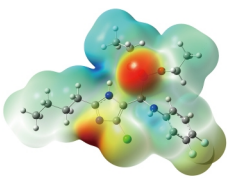

preliminarily study the absorption, distribution, and metabolism.

3.6.1 Absorption spectra of HSA in the presence of compound **3f**

The UV-Vis absorption peak at 278 nm should be attributed to the aromatic rings in Tryptophan (Trp-214), Tyrosine (Tyr-411) and Phenylalanine (Phe) residues in HSA (Figure 9). With the addition of compound **3f**, the peak intensity increased, indicating that **3f** could interact with HSA and the peptide strands of HSA were extended. However, the maximum absorption wavelength remained unchanged, implying that the noncovalent interactions were formed between **3f** and HSA via the π-π stacking between aromatic rings of **3f** and Trp-214, Tyr-411 and Phe residues in the binding cavity of HSA [17].

3.6.2 Fluorescence quenching mechanism with HSA

Fluorescence competition is another approach to explore the binding behaviors of small molecules with HSA. Trp 214 in HSA is a dominant fluorophore capable of fluorescence quenching that absorbs near 280 nm and emits near 340 nm. The emission may be blue-shifted if the group is buried within a native protein, and its emission may be red-shifted when the protein is unfolded. Hence, changes in the fluorescence intensity can reflect the interaction of small molecules with Trp-214 in HSA.

The effect of compound **3f** on the fluorescence intensity to HSA (T=298 K, λ_{ex}=295 nm) was shown in Figure 10. The red solid line was the only emission spectrum of the active small molecule **3f**, which indicated that its fluorescence intensity was very weak and could be negligible in comparison with the fluorescence of HSA at the excitation wavelength. The maximum emission peak of HSA appeared at 348 nm owing to the single Trp-214 residue, exhibiting a regular decrease as the concentration of compound increased, but the maximum emission wavelength of HSA remained unchanged. This suggested that the complexes between **3f** and HSA were formed, and compound **3f** was likely to interact with HSA via the hydrophobic region located in HSA [18]. According to the following well-known Stern-Volmer Eq. (1), the fluorescence quenching data of HSA could be analyzed [20]:

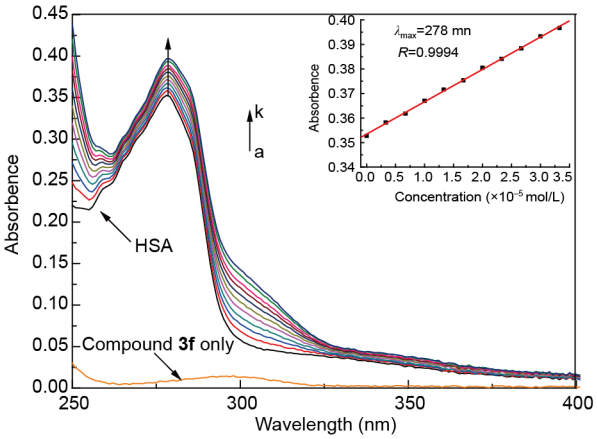

Figure 9 Effect of compound **3f** on HSA UV-Vis absorption. c(HSA)=1.0×10^{-5} mol/L; c(compound **3f**) (×10^{-5} mol/L): (a–k) from 0.0 to 3.33 at the increment of 0.33 (T=298 K, pH 7.4). The inset corresponds to the absorbance at 278 nm with different concentrations of compound **3f** (color online).

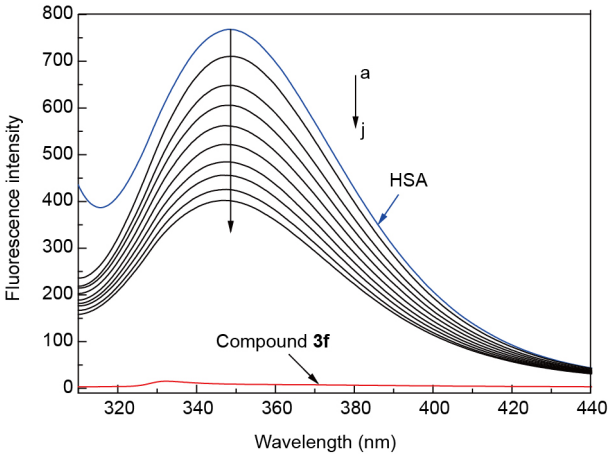

Figure 10 Emission spectra of HSA in the presence of various concentrations of compound **3f**. c(HSA)=1.0×10^{-5} mol/L; c(compound **3f**) (×10^{-5} mol/L): (a–j) from 0.0 to 2.25 at increments of 0.25. Red line shows the emission spectrum of compound **3f** only. T=298 K, λ_{ex}=295 nm (color online).

$$\frac{F_0}{F} = 1 + K_{SV}[Q] = K_q \tau_0 [Q] \quad (1)$$

where F_0 and F represent fluorescence intensity in the absence and presence of compound **3f**, respectively. K_{SV} (L/mol) is the Stern-Volmer quenching constant, [Q] is the concentration of compound **3f**, K_q is the bimolecular quenching rate constant (L/(mol s)), and τ_0 is the fluorescence lifetime of the fluorophore in the absence of quencher, assumed to be 6.4×10^{-9} s for HSA. Hence, the Stern-Volmer plots of HSA in the presence of compound **3f** at different concentrations and temperatures could be calculated and were showed in Figure 11.

Fluorescence quenching occurs by different mechanisms, commonly classified as dynamic quenching and static quenching depending on temperature and viscosity. Higher temperatures usually result in larger diffusion coefficients, and the quenching constants are expected to increase with a gradually increasing temperature in dynamic quenching. However, due to the dissociation of weakly bound complexes, the increasing temperature is likely to result in a smaller static quenching constant.

The values of K_{SV} and K_q for the interaction of compound **3f** with HSA at different temperatures (298, 303, and 310 K) were showed in Table 6. The results indicated that the ground-state complexes were formed between compound **3f** and HSA, and the static quenching governed the quenching

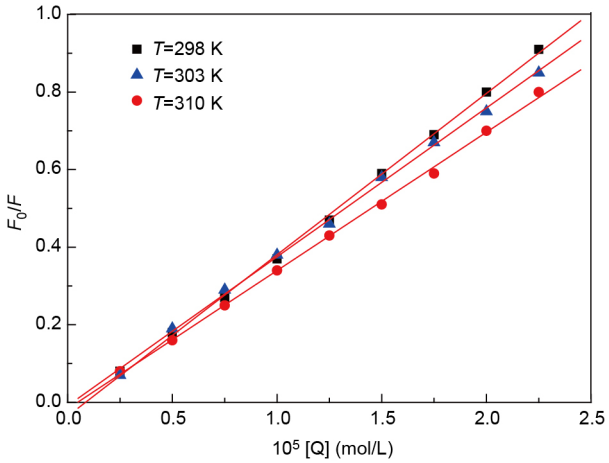

Figure 11 Stern-Volmer plots of **3f**-HSA system at different temperatures (color online).

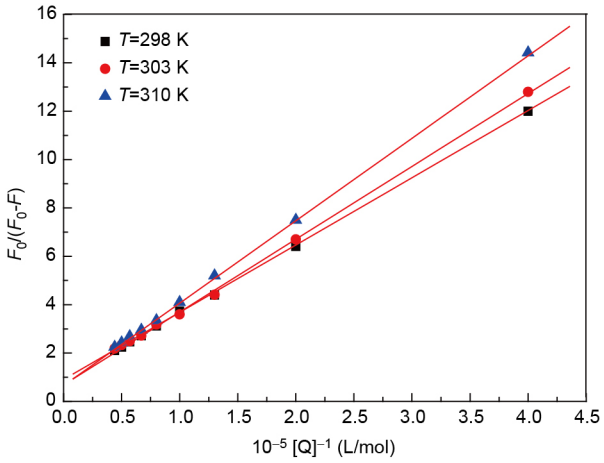

Figure 12 Modified Stern-Volmer plots of **3f**-HSA system at different temperatures (color online).

Table 6 Stern-Volmer quenching constants for the interaction of compound **3f** with HSA at various temperatures

pH	T (K)	K_{SV} (L/mol)	K_q (L/(mol s))	R [a]	S.D. [b]
7.4	298	4.16×10^4	6.50×10^{12}	0.9995	0.010
	303	3.84×10^4	6.00×10^{12}	0.9992	0.115
	310	3.57×10^4	5.58×10^{12}	0.9993	0.010

a) R is the correlation coefficient; b) S.D. is the standard deviation.

mechanism, because the K_q values at different temperatures were in the range of 10^{12} L/(mol s), which far exceeded the diffusion controlled rate constants of various quenchers with a biopolymer (2.0×10^{10} L/(mol s)) [19].

3.6.3 Binding sites and constants

For a static quenching process, the data could be analyzed by the modified Stern-Volmer Eq. (2):

$$\frac{F_0}{\Delta F} = \frac{1}{f_a K_a}\frac{1}{[Q]} + \frac{1}{f_a} \quad (2)$$

where ΔF is the fluorescence difference of HSA in the presence and absence of compound **3f**, and f_a and K_a are the fraction of accessible fluorescence and the effective quenching constant for the accessible fluorophore, respectively. The dependence of $F_0/\Delta F$ on the reciprocal value of the concentration $[Q]^{-1}$, which is linear with the slope equaling to the $(f_aK_a)^{-1}$ value. The modified Stern-Volmer plots were showed in Figure 12 and the calculated results were depicted in Table 7.

The equilibrium binding constant (K_b) and the number of binding sites (n): can be calculated according to the Scatchard Eq. (3):

$$\frac{r}{D_f} = nK_b - rK_b \quad (3)$$

where D_f and r are the molar concentration of free small molecules and the moles of small molecules bound per mole of protein, respectively, n is binding sites multiplicity per class of binding sites, and K_b is the equilibrium binding constant. Figure 13 showed the Scatchard plots, and the binding constants K_b and site n values of the compound **3f**-HSA system were listed in Table 7.

For a static quenching process, the equilibrium binding constant (K_b) and the number of binding site (n) were also calculated (Table 7). The decreased trend of K_a and K_b with increased temperatures was in accordance with the dependence of K_{SV} on temperatures. The value of the binding site n was approximate 1, which showed that one binding site was present in the interaction of **3f** with HSA. The results also showed that the binding constants were suitable and the effects of temperatures were not significant, thus compound **3f** could be stored and transported by HSA.

3.6.4 Binding mode and thermodynamic parameters

It is well-known that there are four types of non-covalent interactions such as hydrogen bonds, electrostatic interactions,

Table 7 Binding constants and sites of **3f**-HSA system at pH 7.4

T (K)	Modified Stern-Volmer method			Scatchard method			
	10^{-4} K_a (L/mol)	R	S.D.	10^{-4} K_b (L/mol)	R	S.D.	n
298	3.25	0.9996	0.091	3.31	0.9965	0.005	1.28
303	2.26	0.9976	0.257	2.27	0.9976	0.020	1.39
310	1.91	0.9995	0.132	2.01	0.9954	0.031	1.41

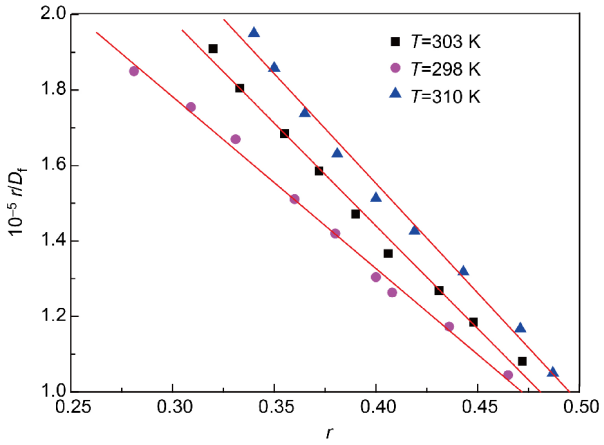

Figure 13 Scatchard plots of **3f**-HSA system at different temperatures (color online).

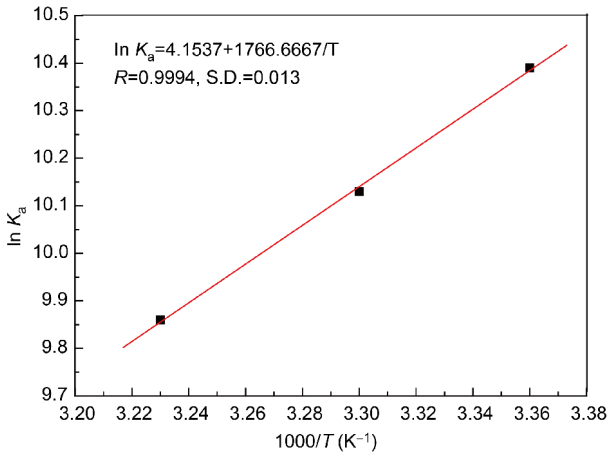

Figure 14 van't Hoff plots of the **3f**-HSA system (color online).

van der Waals forces and hydrophobic bonds, which play important roles in small molecules binding to proteins. The main evidence for confirming the interactions between small molecules and protein is the thermodynamic parameters enthalpy (ΔH) and entropy (ΔS) change of binding reaction. The ΔH and ΔS values can be evaluated from the van't Hoff equation:

$$\ln K = -\frac{\Delta H}{RT} + \frac{\Delta S}{R} \quad (4)$$

where K and R are analogous to the associative binding constants at the corresponding temperature and gas constant, respectively. The thermodynamic parameters were calculated from the van't Hoff plots in order to explain the binding model between compound **3f** and HSA. The ΔH was estimated according to the slope of the van't Hoff relationship in Figure 14. Then, the free energy change (ΔG) was calculated from the following equation:

$$\Delta G = \Delta H - T\Delta S \quad (5)$$

The main evidence to confirm the interactions between small molecules and protein is the thermodynamic parameters enthalpy (ΔH) and entropy (ΔS) change of binding reaction [19]. Herein, $\Delta H<0$ and $\Delta S>0$ obtained in this case indicated that the hydrophobic interactions and hydrogen bonds played important roles in the binding process of compound **3f** and HSA (Table 8).

3.6.5 Synchronous fluorescence spectra

Synchronous fluorescence spectroscopy, a simple and effective technique, was used to explore the molecular microenvironment in the vicinity of the fluorophore in HSA (Figure 15). When the wavelength interval ($\Delta\lambda$) between excitation and emission wavelength was fixed at $\Delta\lambda$=15 nm, the synchronous fluorescence would only exhibit the characteristic spectrum of Tyr-411 residue. If at $\Delta\lambda$=60 nm, it would yield the spectral information of Trp-214 residue. The Tyr-411 fluorescence intensity decreased regularly without no significant change in wavelength with the addition of compound **3f**, indicating that the interactions between **3f** and HSA did not affect the conformation of Tyr-411 micro-region. While there was a blue shift of 4 nm in the maximum emission wavelength (from 285 nm to 281 nm) with gradual decrease in synchronous fluorescence intensity of Trp-214, this indicated that the conformation of HSA was changed and the polarity in the vicinity of Trp-214 residue decreased, leading to the increase of hydrophobicity [20]. Furthermore, as the gradually increased concentration of **3f**, there was a notable decrease in fluorescence intensity at $\Delta\lambda$=60 nm while no appreciable decrease was observed at $\Delta\lambda$=15 nm (Figure 15(C)), which also explained reasonably that compound **3f** had probability to cause conformational changes close to Trp-214 residue rather than Tyr-411.

Table 8 Thermodynamic parameters of **3f**-HSA system at different temperatures

T (K)	ΔH (kJ/mol)	ΔG (kJ/mol)	ΔS (J/(mol K))
298		–24.98	
303	–14.69	–25.15	34.53
310		–25.39	

3.6.6 Energy transfer between HSA and compound **3f**

Förster resonance energy transfer (FRET) theory is typically used to describe energy transfer between donor and acceptor chromophores. According to FRET theory, an excited donor fluorophore can transfer the excited state energy to a nearby acceptor [21]. The non-radioactive energy transfer between drugs and HSA can be explained and determined according to FRET theory. The efficiency of energy transfer is dependent on the extent of overlap between the fluorescence emission spectrum of a donor and the absorption spectrum of an acceptor, the relative angular orientation and the distance between

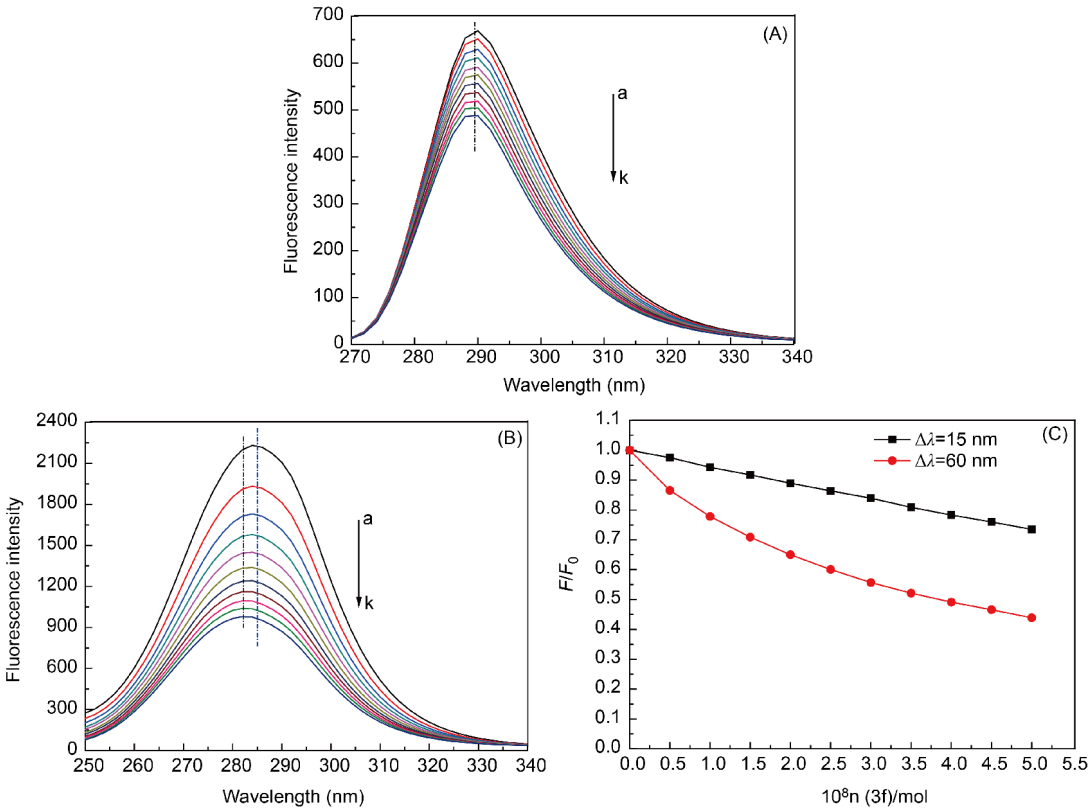

Figure 15 Synchronous fluorescence spectra of HSA in the presence of increasing concentration of **3f**. (A) $\Delta\lambda$=15 nm. (B) $\Delta\lambda$=60 nm.c(HSA)=1.0×10^{-5} mol/L; c(compound **3f**) (10^{-5} mol/L): (a–k) from 0.0 to 2.25 at increments of 0.25. (C) Variation (quenching) curves of relative (F/F_0) synchronous fluorescence intensity of HSA as a function of increasing concentration of **3f** (color online).

donor and acceptor. From the above results, it was established that compound **3f** had probability to cause conformational changes close to Trp-214 residue, which confirmed that **3f** mainly interacted with Trp-214 residue of HSA by non-radioactive energy transfer since there was a suitable spectral overlap between HSA emission and **3f** absorption spectra (Figure 16).

FRET theory is based on a point dipole approximation, namely that the distance between the moieties should be much larger than the size of the individual donor or acceptor dipoles. The efficiency of energy transfer depends on the distance between donor and acceptor, their spectral characteristics, and their relative orientation. In order for transfer to be efficient, the donor and acceptor absorption must be well separated, while the donor emission spectrum must overlap with the absorption of the acceptor. The efficiency of energy E can be evaluated according to Eq. (6):

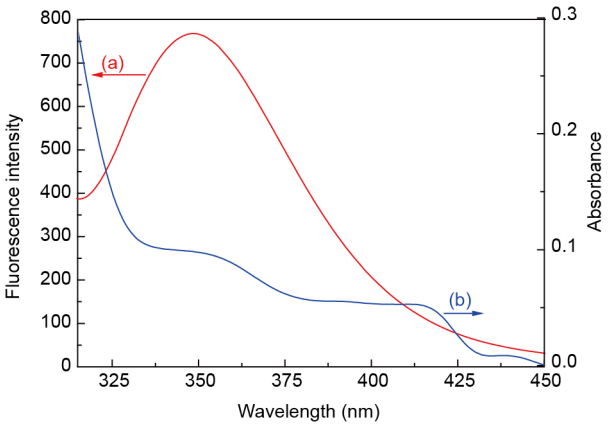

Figure 16 The overlap of fluorescence spectrum of HSA (a) and absorption spectrum of compound **3f** (b). c(HSA)=c(compound **3f**)=1.0×10^{-5} mol/L;T=298 K, pH 7.4 (color online).

$$E = 1 - \frac{F}{F_0} = \frac{R_0^6}{R_0^6 + r_0^6} \tag{6}$$

where R_0 is the Förster distance (critical distance) when the efficiency of energy transfer is 50%, and r_0 is the distance between the donor (HSA) and the acceptor (compound **3f**). F and F_0 are the fluorescence intensity of HSA in the presence and absence of compound **3f**, respectively. R_0 can be calculated from HSA emission and compound **3f** absorption spectra using Eq. (7):

$$R_0^6 = 8.8 \times 10^{-25} K^2 n^{-4} \varphi J \tag{7}$$

where K^2 is the orientation factor related to the geometry of the HSA-**3f** dipole, n is the refractive index of the medium, φ is the fluorescence quantum yield of HSA, and J is the spectral overlap integral between the HSA emission spectrum and the

Table 9 Effect of metal ions on the binding constants of **3f**-HSA complexes at 298 K

Systems	10^{-4} K_a (L/mol)	K_a/K_a^0 a)	R b)	S.D. c)
3f-HSA	3.25	1.00	0.9996	0.091
3f-HSA-K^+	6.33	1.95	0.9999	0.013
3f-HSA-Na^+	6.44	1.98	0.9999	0.031
3f-HSA-Mg^{2+}	5.77	1.77	0.9999	0.037
3f-HSA-Ni^{2+}	5.62	1.73	0.9999	0.032
3f-HSA-Zn^{2+}	7.02	2.16	0.9998	0.047
3f-HSA-Ca^{2+}	5.63	1.73	0.9999	0.033
3f-HSA-Cu^{2+}	7.12	2.19	0.9998	0.038
3f-HSA-Ag^+	7.46	2.30	0.9998	0.038

a) K_a^0 is the binding constant of **3f**-HSA complexes in the absence of metal ions, K_a is the binding constants of **3f**-HSA complexes with metal ions; b) R is the correlation coefficient; c) S.D. is standard deviation.

compound **3f** absorbance spectrum, which was calculated according to Eq. (8). For HSA, K^2, φ, and n were taken as 2/3, 0.118, and 1.33, respectively.

$$J = \frac{\int_0^\infty F(\lambda)\varepsilon(\lambda)\lambda^4\Delta\lambda}{\int_0^\infty F(\lambda)\Delta\lambda} \quad (8)$$

where $F(\lambda)$ is the fluorescence intensity of HSA at wavelength λ, $\varepsilon(\lambda)$ is the molar absorption coefficient of compound **3f** at wavelength λ.

According to the above equations, it could be calculated the spectral overlap integral J=1.01×10^{13} cm^3 L/mol, the efficiency of energy E=0.27, the Förster distance R_0=2.62 nm and the distance between HSA and **3f** r_0=2.96 nm, suggesting that the non-radioactive energy transfer from HSA to **3f** occurred with high possibility based on the prerequisite of $2<r_0<8$ nm [22]. Furthermore, the acquisition of $0.5R_0<r_0<1.5R_0$ indicated that the existence of static quenching due to complex formation between HSA (Trp-214) and compound **3f** [23].

3.6.7 Effect of common metal ions

HSA plays a key role in the transport of metal ions in blood plasma. It is reported that metal ions can form complexes with HSA and then influence drug binding to HSA. Therefore, the effect of the eight metal ions Na^+, K^+, Mg^{2+}, Cu^{2+}, Ca^{2+}, Zn^{2+}, Ni^{2+} and Ag^+ ions on the binding of compound **3f** to HSA was studied at 298 K (Figure S5–Figure S12). It was worthy to note that the competition between the metal ions and **3f** led to the binding constants of HSA-**3f** complexes ranging from 172.9% to 229.5% of the value of binding constant in absence of metal ions (Table 9).

The altered binding constants might be explained by the conformational changes of HSA when bound to metal ions, or the formation of supramolecular interactions between metal ions and **3f**, which in turn affected HSA binding to the agent. Clearly, the presence of the above metal ions increased the binding constants of **3f**-HSA-ions complexes, suggesting the presence of these metal ions could increase the concentration of free compound **3f** and shorten its storage time and half-life in the blood, thus improve the maximum efficacy [24], or possibly produce **3f**-ion supramolecular complexes to exhibit biological activities.

4 Conclusions

In summary, a series of amino organophosphorus imidazoles as a novel type of antimicrobial agents have been successfully developed for the first time. The *in vitro* antimicrobial activities revealed that 3-chloro-4-fluorophenyl derivative **3f** showed superior activities against MRSA and *S. cerevisiae* (MIC=2 μg/mL) to clinical drugs, and its combinations with antibacterial or antifungal drugs enhanced the antimicrobial efficiency. Compound **3f** exhibited low resistant development for bacteria and was membrane-active, but had no significant intercalation towards MRSA DNA. Computational study of **3f** supported its good antimicrobial activity. Experimental data revealed that HSA could form ground-state complexes with **3f** through hydrophobic interactions and hydrogen bonds with the spontaneous binding process, and the non-radioactive energy could transfer from HSA to **3f** beyond FRET theory. Competitive interactions suggested that the participation of K^+, Na^+, Mg^{2+}, Cu^{2+}, Ca^{2+}, Zn^{2+}, Ni^{2+} and Ag^+ ions in **3f**-HSA system could increase the concentration of free compound **3f**, shorten its storage time and half-life in the blood to improve the maximum antimicrobial efficacy, or possibly produce **3f**-ion supramolecular complexes to exhibit biological activities.

Acknowledgments This work was partially supported by the National Natural Science Foundation of China (21672173, 21372186), Research Fund for International Young Scientists from International (Regional) Cooperation and Exchange Program (81350110523), Chongqing Special Foundation for Postdoctoral Research Proposal (Xm2014127, Xm2016039), and Fundamental Research Funds for the Central Universities (XDJK2016E059).

Conflict of interest The authors declare that they have no conflict of interest.

Supporting information The supporting information is available online at http://chem.scichina.com and http://link.springer.com/journal/11426. The supporting materials are published as submitted, without typesetting or editing. The responsibility for scientific accuracy and content remains entirely with the authors.

1 (a) Zhang J, Chen YP, Miller KP, Ganewatta MS, Bam M, Yan Y, Nagarkatti M, Decho AW, Tang C. *J Am Chem Soc*, 2014, 136: 4873–4876; (b) Oh D, Sun J, Nasrolahi Shirazi A, LaPlante KL, Rowley DC, Parang K. *Mol Pharm*, 2014, 11: 3528–3536; (c) Zhou CH, Wang Y. *Curr Med Chem*, 2012, 19: 239–280; (d) Wang H, Jeyakkumar P, Nagarajan S, Meng JP, Zhou CH. *Prog Chem*, 2015, 27: 704–743; (e) Wang XL, Wan K, Zhou CH. *Eur J Med Chem*, 2010, 45: 4631–4639

2 (a) Zhang L, Peng XM, Damu GLV, Geng RX, Zhou CH. *Med Res Rev*, 2014, 34: 340–437; (b) Pieczonka AM, Strzelczyk A, Sadowska B, Mlostoń G, Stączek P. *Eur J Med Chem*, 2013, 64: 389–395; (c) Peng XM, Damu GLV, Zhou CH. *Curr Pharm Des*, 2013, 19: 3884–3930; (d) Peng XM, Cai GX, Zhou CH. *Curr Top Med Chem*, 2013, 13: 1963–2010

3 (a) Wen SQ, Jeyakkumar P, Avula SR, Zhang L, Zhou CH. *Bioorg Med Chem Lett*, 2016, 26: 2768–2773; (b) Peng XM, Peng LP, Li S, Avula SR, Kannekanti VK, Zhang SL, Tam KY, Zhou CH. *Future Med Chem*, 2016, 8: 1927–1940; (c) Gong HH, Baathulaa K, Lv JS, Cai GX, Zhou CH. *Med Chem Commun*, 2016, 7: 924–931; (d) Gong HH, Addla D, Lv JS, Zhou CH. *Curr Top Med Chem*, 2016, 16: 3303–3364

4 (a) Falagas ME, Kastoris AC, Karageorgopoulos DE, Rafailidis PI. *Int J Antimicrob Agents*, 2009, 34: 111–120; (b) Hirsch EB, Raux BR, Zucchi PC, Kim Y, McCoy C, Kirby JE, Wright SB, Eliopoulos GM. *Int J Antimicrob Agents*, 2015, 46: 642–647; (c) Faísca Phillips AM, Barros MT, Pacheco M, Dias R. *Bioorg Med Chem Lett*, 2014, 24: 49–53; (d) Aoyama T, Hirata K, Hirata R, Yamazaki H, Yamamoto Y, Hayashi H, Matsumoto Y. *J Clin Pharm Ther*, 2012, 37: 356–363; (e) Hecker SJ, Erion MD. *J Med Chem*, 2008, 51: 2328–2345

5 (a) Zhang HZ, Jeyakkumar P, Vijaya Kumar K, Zhou CH. *New J Chem*, 2015, 39: 5776–5796; (b) Zhang L, Kumar KV, Rasheed S, Geng RX, Zhou CH. *Chem Biol Drug Des*, 2015, 86: 648–655; (c) Damu GLV, Wang QP, Zhang HZ, Zhang YY, Lv JS, Zhou CH. *Sci China Chem*, 2013, 56: 952–969; (d) Jeyakkumar P, Zhang L, Avula SR, Zhou CH. *Eur J Med Chem*, 2016, 122: 205–215

6 (a) Vijesh AM, Isloor AM, Telkar S, Arulmoli T, Fun HK. *Arab J Chem*, 2013, 6: 197–204; (b) Zhang L, Addla D, Ponmani J, Wang A, Xie D, Wang YN, Zhang SL, Geng RX, Cai GX, Li S, Zhou CH. *Eur J Med Chem*, 2016, 111: 160–182; (c) Dai LL, Zhang HZ, Nagarajan S, Rasheed S, Zhou CH. *Med Chem Commun*, 2015, 6: 147–154; (d) Wang Y, Damu GLV, Lv JS, Geng RX, Yang DC, Zhou CH. *Bioorg Med Chem Lett*, 2012, 22: 5363–5366; (e) Cheng Y, Wang H, Addla D, Zhou C. *Chin J Org Chem*, 2016, 36: 1–42

7 (a) Zghab I, Trimeche B, Besbes M, Touboul D, Martin MT, Jannet HB. *Med Chem Res*, 2015, 24: 2167–2176; (b) Demkowicz S, Rachon J, Daśko M, Kozak W. *RSC Adv*, 2016, 6: 7101–7112; (c) Reddy CB, Kumar KS, Kumar MA, Narayana Reddy MV, Krishna BS, Naveen M, Arunasree MK, Reddy CS, Raju CN, Reddy CD. *Eur J Med Chem*, 2012, 47: 553–559; (d) Demmer CS, Krogsgaard-Larsen N, Bunch L. *Chem Rev*, 2011, 111: 7981–8006

8 (a) Ensign SC, Vanable EP, Kortman GD, Weir LJ, Hull KL. *J Am Chem Soc*, 2015, 137: 13748–13751; (b) Addla D, Wen SQ, Gao WW, Maddili SK, Zhang L, Zhou CH. *Med Chem Commun*, 2016, 7: 1988–1994; (c) Jeyakkumar P, Liu HB, Gopala L, Cheng Y, Peng XM, Geng RX, Zhou CH. *Bioorg Med Chem Lett*, 2017, 27: 1737–1743

9 (a) Chellat MF, Raguž L, Riedl R. *Angew Chem Int Ed*, 2016, 55: 6600–6626; (b) Kharb R, Tyagi M, Sharma AK. *Pharma Chem*, 2014, 6: 298–320

10 (a) Zhang RR, Liu J, Zhang Y, Hou MQ, Zhang MZ, Zhou F, Zhang WH. *Eur J Med Chem*, 2016, 116: 76–83; (b) Peng XM, Kumar KV, Damu GLV, Zhou CH. *Sci China Chem*, 2016, 59: 878–894; (c) Damu GLV, Cui SF, Peng XM, Wen QM, Cai GX, Zhou CH. *Bioorg Med Chem Lett*, 2014, 24: 3605–3608

11 National Committee for Clinical Laboratory Standards Approved standard Document. M27-A2. Reference Method for Broth Dilution Antifungal Susceptibility Testing of Yeasts. Wayne, PA: National Committee for Clinical Laboratory Standards, 2002

12 (a) Rosato A, Piarulli M, Corbo F, Muraglia M, Carone A, Vitali M, Vitali C. *Curr Med Chem*, 2010, 17: 3289–3295; (b) Zhang HZ, Damu GLV, Cai GX, Zhou CH. *Eur J Med Chem*, 2013, 64: 329–344

13 (a) Kim HY, Wiles JA, Wang Q, Pais GCG, Lucien E, Hashimoto A, Nelson DM, Thanassi JA, Podos SD, Deshpande M, Pucci MJ, Bradbury BJ. *J Med Chem*, 2011, 54: 3268–3282; (b) Lohan S, Cameotra SS, Bisht GS. *Eur J Med Chem*, 2014, 83: 102–115

14 (a) Negi B, Kumar D, Kumbukgolla W, Jayaweera S, Ponnan P, Singh R, Agarwal S, Rawat DS. *Eur J Med Chem*, 2016, 115: 426–437; (b) Tan H, Liu H, Zhao L, Yuan Y, Li B, Jiang Y, Gong L, Qiu S. *Eur J Med Chem*, 2017, 125: 492–499

15 (a) Ghosh C, Manjunath GB, Akkapeddi P, Yarlagadda V, Hoque J, Uppu DSSM, Konai MM, Haldar J. *J Med Chem*, 2014, 57: 1428–1436; (b) Konai MM, Ghosh C, Yarlagadda V, Samaddar S, Haldar J. *J Med Chem*, 2014, 57: 9409–9423; (c) Fang XJ, Jeyakkumar P, Avula SR, Zhou Q, Zhou CH. *Bioorg Med Chem Lett*, 2016, 26: 2584–2588

16 (a) Cheng Y, Avula SR, Gao WW, Addla D, Tangadanchu VKR, Zhang L, Lin JM, Zhou CH. *Eur J Med Chem*, 2016, 124: 935–945; (b) Cui SF, Addla D, Zhou CH. *J Med Chem*, 2016, 59: 4488–4510

17 (a) Suryawanshi VD, Anbhule PV, Gore AH, Patil SR, Kolekar GB. *Ind Eng Chem Res*, 2012, 51: 95–102; (b) Zhang SL, Damu GLV, Zhang L, Geng RX, Zhou CH. *Eur J Med Chem*, 2012, 55: 164–175

18 (a) Peng LP, Nagarajan S, Rasheed S, Zhou CH. *Med Chem Commun*, 2015, 6: 222–229; (b) Zhang L, Chang JJ, Zhang SL, Damu GLV, Geng RX, Zhou CH. *Bioorg Med Chem*, 2013, 21: 4158–4169

19 (a) Yin BT, Yan CY, Peng XM, Zhang SL, Rasheed S, Geng RX, Zhou CH. *Eur J Med Chem*, 2014, 71: 148–159; (b) Cui SF, Ren Y, Zhang SL, Peng XM, Damu GLV, Geng RX, Zhou CH. *Bioorg Med Chem Lett*, 2013, 23: 3267–3272

20 (a) Varlan A, Hillebrand M. *Molecules*, 2010, 15: 3905–3919; (b) Liu B, Guo Y, Wang J, Xu R, Wang X, Wang D, Zhang L, Xu Y. *J Luminescence*, 2010, 130: 1036–1043

21 (a) Nelson T, Fernandez-Alberti S, Roitberg AE, Tretiak S. *Phys Chem Chem Phys*, 2013, 15: 9245–9256; (b) Kim H, Abeysirigunawarden SC, Chen K, Mayerle M, Ragunathan K, Luthey-Schulten Z, Ha T, Woodson SA. *Nature*, 2014, 506: 334–338

22 (a) Fudo S, Yamamoto N, Nukaga M, Odagiri T, Tashiro M, Neya S, Hoshino T. *Bioorg Med Chem*, 2015, 23: 5466–5475; (b) Li Y, You L, Huang W, Liu J, Zhu H, He B. *Eur J Med Chem*, 2015, 96: 245–249

23 (a) Li Y, You L, Huang W, Liu J, Zhu H, He B. *Eur J Med Chem*, 2015, 96: 245–249; (b) Bio M, Rajaputra P, You Y. *Bioorg Med Chem Lett*, 2016, 26: 145–148

24 (a) Cui SF, Peng LP, Zhang HZ, Rasheed S, Vijaya Kumar K, Zhou CH. *Eur J Med Chem*, 2014, 86: 318–334; (b) Zhang SL, Chang JJ, Damu GLV, Fang B, Zhou XD, Geng RX, Zhou CH. *Bioorg Med Chem Lett*, 2013, 23: 1008–1012